

# Quantum delayed-choice experiment with a beam splitter in a quantum superposition

Shi-Biao Zheng<sup>1,\*</sup>, You-Peng Zhong<sup>2</sup>, Kai Xu<sup>2</sup>, Qi-Jue Wang<sup>2</sup>, H. Wang<sup>2</sup>, Li-Tuo Shen<sup>1</sup>,  
Chui-Ping Yang<sup>3</sup>, John M. Martinis<sup>4,†</sup>, A. N. Cleland<sup>5,‡</sup> and Si-Yuan Han<sup>6,7</sup>

<sup>1</sup> *Department of Physics, Fuzhou University, Fuzhou 350116, China*

<sup>2</sup> *Department of Physics, Zhejiang University, Hangzhou 310027, China*

<sup>3</sup> *Department of Physics, Hangzhou Normal University, Hangzhou 310036, China*

<sup>4</sup> *Department of Physics, University of California, Santa Barbara, California 93106, USA*

<sup>5</sup> *Institute for Molecular Engineering, University of Chicago, Chicago, Illinois 60637, USA*

<sup>6</sup> *Department of Physics and Astronomy, University of Kansas, Lawrence, Kansas 66045, USA*

<sup>7</sup> *Beijing National Laboratory for Condensed Matter Physics,  
Institute of Physics, Chinese Academy of Sciences, Beijing 100190, China*

A quantum system can behave as a wave or as a particle, depending on the experimental arrangement. When for example measuring a photon using a Mach-Zehnder interferometer, the photon acts as a wave if the second beam-splitter is inserted, but as a particle if this beam-splitter is omitted. The decision of whether or not to insert this beam-splitter can be made after the photon has entered the interferometer, as in Wheeler’s famous delayed-choice thought experiment. In recent quantum versions of this experiment, this decision is controlled by a quantum ancilla, while the beam splitter is itself still a classical object. Here we propose and realize a variant of the quantum delayed-choice experiment. We configure a superconducting quantum circuit as a Ramsey interferometer, where the element that acts as the first beam-splitter can be put in a quantum superposition of its active and inactive states, as verified by the negative values of its Wigner function. We show that this enables the wave and particle aspects of the system to be observed with a single setup, without involving an ancilla that is not itself a part of the interferometer. We also study the transition of this quantum beam-splitter from a quantum to a classical object due to decoherence, as observed by monitoring the interferometer output.

PACS numbers: 03.65.Ta; 42.50.St; 42.50.Dv

The wave-particle duality is one of the fundamental mysteries that lie at the heart of quantum mechanics. However, these two incompatible aspects cannot be observed simultaneously, as captured by Bohr’s principle of complementarity [1 – 5]: Particle-like versus wave-like outcomes are selected by experimental arrangements that are mutually exclusive. This is well illustrated by the Mach-Zehnder interferometer, as shown in Fig. 1(a). Split by the first beam splitter ( $BS_1$ ), a photon travels along two paths, 0 and 1. The relative phase  $\theta$  between the quantum states associated with these paths is tunable. In the presence of the second beam splitter ( $BS_2$ ), the two paths are recombined and the probability for detecting the photon in the detector  $D_0$  or  $D_1$  is a sinusoidal function of  $\theta$ , exhibiting wave-like interference fringes. On the other hand, in the absence of  $BS_2$ , the experiment reveals which path the photon followed, and the photon is detected in one or the other detector with equal probability  $1/2$ , thus behaving as a particle.

One can argue that the behavior of the photon is pre-determined by the experimental arrangement, where the presence or absence of the second beam splitter affects the photon prior to its entering the interferometer. The possibility of such a causal link is precluded in Wheeler’s delayed-choice experiment [6 – 8], in which the observer randomly chooses whether to insert  $BS_2$ , and thus whether to perform an interference or a which-path experiment, after the photon has passed

through  $BS_1$ . Therefore, the photon could not “know” in advance which behavior it should exhibit. Wheeler’s delayed-choice experiment has been demonstrated previously [9 – 13], where the space-like separation between the setup selection and the photon entry into the interferometer was achieved in Ref. [12]. Recently, a quantum version of the delayed-choice experiment was suggested [14], in which the action of  $BS_2$  is controlled by a quantum ancilla. The scheme is illustrated in Fig. 1(b), where each beam splitter is replaced by a Hadamard operation  $H$ , and the second Hadamard operation is conditionally applied following the phase shift  $\theta$ . The quantum system exhibits wave-like behavior if the ancilla is in its  $|1\rangle$  state and the second Hadamard is applied; if the ancilla is instead in  $|0\rangle$ , the second Hadamard is not performed, and the system displays particle-like behavior. When the ancilla is prepared in a superposition of  $|0\rangle$  and  $|1\rangle$ , the result is a superposition of wave-like and particle-like states, entangled with the ancilla [14]. This clearly precludes the system ‘knowing’ in advance which setup will be selected; the quantum superposition effectively replaces the need for Wheeler’s space-like separation of the photon entry into the interferometer and the measurement selection. Instead, the wave-like and particle-like behaviors are post-selected by measuring the ancilla in its  $(|0\rangle, |1\rangle)$  basis. This allows the complementary wave and particle behaviors to emerge from a single experimental set-up, showing that the complementarity really

resides in the experimental data, rather than resulting from the experiment's physical arrangement.

Quantum delayed-choice experiments have been performed in both NMR [15, 16] and optical systems [17 – 19]. In the optical experiments reported in Refs. [18] and [19], the quantum correlation between the test photon and the quantum ancilla was verified by the violation of a Bell inequality; we note that these measurements are subject to the fair-sampling assumption, that is, the large number of coincident photon pairs that fail to be registered are assumed to obey the same statistics as those that are recorded.

Here we theoretically propose and experimentally implement a variant of the quantum delayed-choice experiment, using a superconducting Ramsey interferometer and the process shown in Fig. 1(c); we note that the Ramsey and Mach-Zehnder interferometers are physically different, but actually implement the same quantum circuit [20]. In our interferometer, a two-level quantum system (a superconducting qubit), with ground state  $|g\rangle$  and excited state  $|e\rangle$ , which correspond to the paths 0 and 1 in the optical interferometer, is subjected to two Ramsey rotations,  $R_1$  and  $R_2(\theta)$ , which correspond to the two beam-splitters of the Mach-Zehnder interferometer but are induced by microwave fields. The tunable phase shift  $\theta$  between the two interfering paths is incorporated into the microwave field that produces  $R_2(\theta)$ .  $R_1$  is generated by the microwave field stored in a superconducting resonator. If the resonator is “filled” by exciting it into the appropriate microwave coherent state  $|\alpha\rangle$ , the qubit will undergo a Hadamard transformation by interacting with this field. This rotates the input state from  $|g\rangle$  into a superposition of  $|g\rangle$  and  $|e\rangle$ , producing two paths in the Hilbert space, as with the first beam-splitter in the Mach-Zehnder interferometer. These two paths are then recombined by  $R_2(\theta)$ , and that recombination results in  $\theta$ -dependent wave-like interference fringes in the probabilities of  $|g\rangle$  and  $|e\rangle$ . If the resonator is instead “empty”, i.e. in its ground state  $|0\rangle$ , no rotation  $R_1$  occurs, and the qubit remains in  $|g\rangle$ . The second rotation  $R_2(\theta)$  then produces a superposition of  $|g\rangle$  and  $|e\rangle$ , but the probabilities of  $|g\rangle$  and  $|e\rangle$  have no  $\theta$  dependence, corresponding to particle-like behavior. We note that the required conditional dynamics cannot be realized when the order of the two rotations in Fig. 1(c) is inverted: To realize the resonator-state-dependent rotation, the qubit should be in the state  $|g\rangle$  before interaction with the resonator, so that the resonator's ground state  $|0\rangle$  cannot induce any rotation on the qubit; however, when the unconditional rotation  $R_2(\theta)$  is applied first, before the qubit-resonator interaction the qubit has a probability of  $1/2$  to be excited by  $R_2(\theta)$  to the state  $|e\rangle$ , to which the resonator's ground state can produce a rotation through the vacuum Rabi oscillation [24].

The wave and particle behavior of the qubit can be investigated simultaneously by preparing the resonator in

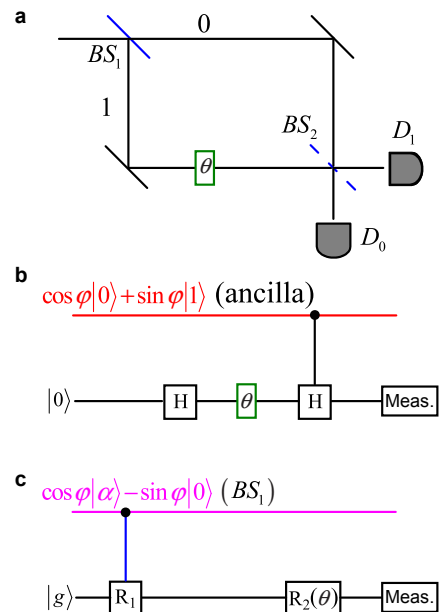


FIG. 1: (Color online) (a) Schematic of Wheeler's delayed-choice thought experiment. A photon's state is transformed by the first beam splitter  $BS_1$ , into a superposition of two paths, 0 and 1, followed by a tunable phase shift  $\theta$ . While the photon is inside the interferometer, the observer decides whether or not to insert a second beam splitter  $BS_2$ , thereby delaying the decision of whether to measure an interference pattern (wave aspect) or to obtain which-path information (particle aspect), as revealed by the probability of detecting the photon at detector  $D_0$  and  $D_1$  as a function of  $\theta$ . (b) Schematic of the quantum delayed-choice experiment using a controlling quantum ancilla. The effect of each beam splitter is represented by a Hadamard operation  $H$ , with the relative phase shift  $\theta$  occurring in-between these two operations. The second Hadamard is controlled by the ancilla, which can be prepared in a superposition state, allowing simultaneous preparation of the wave and particle aspects of the test system. (c) Schematic of the delayed choice experiment, implemented with a superconducting beam splitter that is put into a cat-like superposition state. The test qubit, initially in the ground state  $|g\rangle$ , is subjected to two operations,  $R_1$  and  $R_2(\theta)$ , equivalent in combination to the two Hadamard operations plus the phase shift  $\theta$ .  $R_1$  is implemented (active) when the test qubit interacts with a superconducting resonator occupied by a classical coherent field  $|\alpha\rangle$ .  $R_2(\theta)$  is implemented by a classical microwave pulse. The final probability of measuring the qubit in the ground state  $|g\rangle$  or excited state  $|e\rangle$ , for active  $R_1$ , then depends on the relative phase  $\theta$ , thus exhibiting Ramsey interference. When the superconducting resonator is instead in the ground state  $|0\rangle$ ,  $R_1$  is not implemented (inactive), and no  $\theta$ -dependent Ramsey interference occurs. The wave and particle aspects of the qubit can be superposed by preparing the resonator in a quantum superposition of "filled"  $|\alpha\rangle$  and "empty"  $|0\rangle$  states, generating an output state that encodes both particle- and wave-like behavior.

a superposition of its “filled”  $|\alpha\rangle$  and “empty”  $|0\rangle$  states, i.e. in a Schrödinger cat state [21]. The nonclassical nature of this quantum beam splitter (QBS) can be revealed by measuring the negative values of its Wigner function (WF) [22], which is the resonator’s quasiprobability distribution in phase space. This enables one to verify the existence of a coherent quantum superposition of the filled and empty, or active and inactive, states of the QBS, without performing a Bell measurement. In this case, after  $R_2$ , the wave and particle states of the qubit are entangled with the state of the resonator. This is in contrast to previous realizations of quantum delayed-choice experiments [15 – 19], where the wave-particle response of the quantum system is determined by the state of a quantum ancilla, which is not itself a part of the interferometer, but instead determines the action (or inaction) of one of the two beam-splitters. In these experiments, the test system is entangled with the ancilla through the conditional action of the beam-splitter, while the beam splitter remains a fully classical object. With our setup, we can also investigate the transition of the QBS to a classical beam-splitter due to its intrinsic environmentally-induced decoherence. As far as we know, this is the first interference experiment in which one beam splitter in an interferometer is in a coherent superposition of its active and inactive states. We note that our setup, using a temporally-based Ramsey interferometer, does not permit the space-like separation required for Wheeler’s original gedanken experiment.

The rotation  $R_1$  of the qubit is produced by the microwave field stored in the resonator, which is resonantly coupled to the qubit transition  $|g\rangle \leftrightarrow |e\rangle$  with coupling strength  $\Omega$ . If the resonator is in the state  $|\alpha\rangle$ , a coherent microwave photon state with amplitude  $\alpha$  and mean photon number  $\langle n \rangle = |\alpha|^2$ , the qubit exchanges energy with the resonator and Rabi-oscillates between  $|g\rangle$  and  $|e\rangle$ . For simplicity, we assume  $\alpha$  is real and positive. When  $\alpha \gg 1$ , after an interaction time  $t_\alpha = \pi/(4\alpha\Omega)$ , the qubit state is approximately  $|\psi_\alpha\rangle = (|g\rangle - i|e\rangle)/\sqrt{2}$ , with the resonator field left close to its original state  $|\alpha\rangle$ . Numerical simulation shows that the approximation is good even for moderate values of  $\alpha$ . This result has a simple qualitative explanation: When the resonator’s coherent field is not too weak, its Poissonian photon-number distribution and hence its state is insensitive to a one-photon change. If the resonator is instead in its ground state  $|0\rangle$ , the rotation  $R_1$  does not occur and the qubit remains in  $|g\rangle$ . The second pulse  $R_2(\theta)$ , generated by a classical microwave pulse, performs the transformations  $|g\rangle \rightarrow (|g\rangle - ie^{-i\theta}|e\rangle)/\sqrt{2}$  and  $|e\rangle \rightarrow (|e\rangle - ie^{i\theta}|g\rangle)/\sqrt{2}$ . When acting on the state  $|\psi_\alpha\rangle$ , this results in the state

$$|\psi_w\rangle = -i \left[ \sin(\theta/2)e^{i\theta/2}|g\rangle + \cos(\theta/2)e^{-i\theta/2}|e\rangle \right]. \quad (1)$$

The probability of measuring the qubit in  $|e\rangle$  is then  $\cos^2(\theta/2)$ , showing the  $\theta$ -dependent interference associ-

ated with wave-like behavior. If  $R_1$  did not occur, due to the microwave resonator being in its ground state  $|0\rangle$ , the final state after the second rotation  $R_2$  is

$$|\psi_p\rangle = (|g\rangle - ie^{-i\theta}|e\rangle)/\sqrt{2}. \quad (2)$$

The probability to be in  $|g\rangle$  or  $|e\rangle$  is 1/2, representing particle-like behavior without the  $\theta$ -dependent interference effects.

Now we suppose that the resonator is instead initially prepared in a cat state

$$|\psi_{b,i}\rangle = \mathcal{N}(\cos\varphi|\alpha\rangle - \sin\varphi|0\rangle), \quad (3)$$

where  $\mathcal{N} = \left[1 - e^{-|\alpha|^2/2} \sin(2\varphi)\right]^{-1/2}$ . After the two rotations  $R_1$  and  $R_2(\theta)$ , the qubit-QBS system will then approximately be in the entangled state

$$|\psi_{q+b,f}\rangle \simeq \mathcal{N}_t(\cos\varphi|\psi_w\rangle|\alpha\rangle - \sin\varphi|\psi_p\rangle|0\rangle), \quad (4)$$

where  $\mathcal{N}_t = \left[1 - e^{-|\alpha|^2/2} \sin(2\varphi)/\sqrt{2}\right]^{-1/2}$ . The probability  $P_e$  for finding the qubit in the state  $|e\rangle$  is then close to

$$P_e \simeq \mathcal{N}_t^2 \left[ \frac{1}{2} \sin^2\varphi + \cos^2\varphi \cos^2\frac{\theta}{2} \right]. \quad (5)$$

The Ramsey interference pattern thus simultaneously exhibits the wave and particle behaviors, through the presence and absence, respectively, of  $\theta$  dependence in the two terms that make up  $P_e$ . The quantum coherence between the two state components  $|\alpha\rangle$  and  $|0\rangle$  precludes the possibility of the qubit “knowing” in advance what type of experiment will be performed. We note that for  $\varphi = 0$  this interferometer is equivalent to the cavity QED analogue described in Ref. [5] except there the qubit is initially in  $|e\rangle$ .

The detailed implementation of this quantum delayed-choice experiment involves a superconducting resonator and two tunable superconducting phase qubits, one qubit serving as the test qubit and the second control qubit used to program the state of the superconducting resonator, as well as to read out the resonator at the end of each experiment. The two qubits are coupled to the resonator with on-resonance coupling strengths  $\Omega$  and  $\Omega'$ , respectively, and the effective coupling of each qubit to the resonator can be effectively switched on or off by tuning the qubit on- or off-resonance with the resonator. The experimental apparatus is identical to that described in Ref. [23]. Using this apparatus, we can arrive at the state  $|\psi_{b,i}\rangle$  of Eq. (3) with  $\alpha = 2$ , and arbitrary values of  $\varphi$  (Ref. [24]; see Supplementary Material). For  $\varphi = \pi/4$ , the fidelity  $F = \langle \psi_{b,i} | \rho_{b,i} | \psi_{b,i} \rangle = 0.726 \pm 0.028$  ( $\rho_{b,i}$  is the density operator corresponding to the output state). It would be preferable to obtain states with larger photon amplitude  $\alpha$ , but we are limited by the small nonlinearity

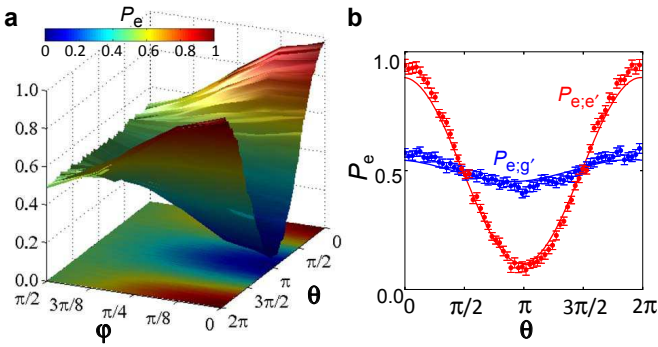


FIG. 2: (Color online) Measured Ramsey interference signal. (a) Probability  $P_e$ , defined in Eq. (5), versus  $\theta$  and  $\varphi$ . The amplitude of the coherent state component of the cat state  $|\psi_{b,i}\rangle$  is  $\alpha = 2$ . The transition between the wave and particle behaviors is clearly apparent. (b) Probabilities  $P_{e;e'}$  and  $P_{e;g'}$ , versus  $\theta$ , for detecting the test qubit in  $|e\rangle$  given that the control qubit is detected in  $|e'\rangle$  and  $|g'\rangle$ , respectively. The control qubit's state reflects the QBS state, as this qubit is measured after it has interacted with the post- $R_2$  resonator state for a time  $\pi/(2\alpha\Omega')$ . Data are for  $\varphi = \pi/4$ . Error bars indicate the statistical variance. Lines are simulations taking into account imperfections in preparing  $|\psi_{b,i}\rangle$ .

of our phase qubits to  $\alpha \lesssim 2$ . Fortunately, numerical simulations show that the overlap between the final qubit-QBS state and  $|\psi_{q+b,f}\rangle$  of Eq. (4) is higher than 0.98 even for this value of  $\alpha$  (ignoring experimental imperfections). After generating  $|\psi_{b,i}\rangle$ , we resonantly couple the test qubit to the resonator for a time  $t_\alpha$ , and then apply a carefully tuned, on-resonance microwave  $\pi/2$  pulse to the qubit, thus implementing the rotation  $R_2(\theta)$ . Figure 2(a) displays the measured probability  $P_e$  as a function of  $\theta$  and  $\varphi$ , which clearly demonstrates the morphing between particle and wave behavior. To more precisely understand this behavior, we need to examine the state of the QBS. This is achieved using the control qubit, initially in the state  $|g'\rangle$ , and tuning it into resonance with the resonator for a time  $\pi/(2\alpha\Omega')$ . If the resonator contains a coherent field  $|\alpha\rangle$ , the control qubit will absorb a photon and undergo the transition  $|g'\rangle \rightarrow |e'\rangle$ , while if the resonator is in  $|0\rangle$ , the qubit remains in  $|g'\rangle$ . The test qubit behavior is post-selected by correlating its measurements with the outcomes of the control qubit measurements. We note that  $|\alpha\rangle$  is not strictly orthogonal to  $|0\rangle$ , with the overlap  $|\langle\alpha|0\rangle|^2 \approx 10^{-2}$  for  $\alpha = 2$ , so that these two components cannot be unambiguously discriminated; there is a small probability that the detection of  $|0\rangle$  actually comes from  $|\alpha\rangle$ . With  $\alpha$  somewhat larger, this overlap will become negligible: For  $\alpha = 3$ , this probability is only about  $10^{-4}$ .

Figure 2(b) shows the measured probabilities  $P_{e;e'}$  and  $P_{e;g'}$  for detecting the test qubit in the state  $|e\rangle$  conditioned upon the detection of the control qubit in  $|e'\rangle$  and  $|g'\rangle$ , respectively; these are measured as a function of  $\theta$ . Here the parameter  $\varphi$  is  $\pi/4$ , corresponding to the QBS

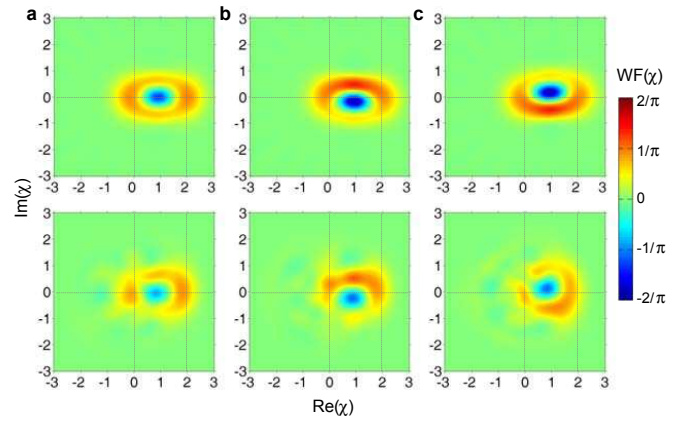


FIG. 3: (Color online) Wigner tomography of the quantum beam splitter. The parameters are  $\alpha = 2$ ,  $\theta = \pi/2$  and  $\varphi = \pi/4$ . The quantum beam splitter Wigner functions (WFs) are displayed for three cases: (a) Test qubit state is not read out; (b) Test qubit is measured in  $|g\rangle$ ; (c) Test qubit is measured in  $|e\rangle$ . The simulated and measured WF's are shown in the upper and lower rows, respectively, as a function of the coordinate  $x$  in resonator phase space. Experimental imperfections are not included in the numerical simulations. The minimum values of the three measured WF's are  $-0.258 \pm 0.030$ ,  $-0.342 \pm 0.027$ , and  $-0.336 \pm 0.028$ , respectively.

being in an equal superposition of its active and inactive states. As expected,  $P_{e;e'}$  exhibits Ramsey interference fringes, with the contrast reaching 0.839, while  $P_{e;g'}$  remains almost constant. The slight oscillations in  $P_{e;g'}$  are mainly due to the fact that the amplitude of the coherent state component  $|\alpha\rangle$  is somewhat small, so that the control qubit has a small probability of remaining in the ground state after the interaction even when the resonator is in  $|\alpha\rangle$ . On one hand, the coherent state contains a vacuum state component, which is decoupled from the qubit state  $|g'\rangle$ . On the other hand, not all the other superposed Fock states can make the control qubit flip to the excited state  $|e'\rangle$  with a unity probability after the interaction, owing to the photon-number dependence of the Rabi frequency. These two reasons account for the  $\theta$ -dependent interference effect in  $P_{e;g'}$ , with a fringe contrast measured to be 0.19. It is noted that taking into account the imperfect initial state as we prepared experimentally, we could verify that the measured fringe data (dots with error bars) are in good agreement with the numerical simulation (lines) in Fig. 2(b). With an increase in the coherent state amplitude  $\alpha$ , the state  $|\alpha\rangle$  is more clearly distinguished from  $|0\rangle$ , and as a result the unwanted oscillations decay dramatically: For  $\alpha = 3$ , the calculated fringe contrast is reduced to 0.017.

It should be noted that the same statistical data can be produced if the resonator field is in the classical mixture  $\cos^2 \varphi |\alpha\rangle\langle\alpha| + \sin^2 \varphi |0\rangle\langle 0|$ . To exclude the classical interpretation, the existence of quantum coherence

between  $|\alpha\rangle$  and  $|0\rangle$  should be verified. The quantum state of the resonator field can be characterized by measuring its Wigner function (WF)  $W(\chi)$ , which describes the quasiprobability distribution of the microwave field in resonator phase space [22]. The WF associated with the density operator  $\rho_b$  is defined as

$$W(\chi) = \frac{2}{\pi} \text{Tr} \left[ e^{i\pi a^\dagger a} D(-\chi) \rho_b D(\chi) \right], \quad (6)$$

where  $\chi$  is the (complex) coordinate in phase space, and  $D$  is the displacement operator. This quantity is always non-negative for the QBS in a classical mixture; the observation of negative values in regions of phase space is a signature of quantum interference. The Wigner function of the QBS was measured using the control qubit, following the procedure developed in Ref. [24]. In Fig. 3(a), we display the WF after performing the second rotation  $R_2(\theta)$ , but without reading out the state of the test qubit, while in Figs. 3(b) and (c) we show the WFs measured with the test qubit having been measured in  $|g\rangle$  and  $|e\rangle$ , respectively, all for  $\theta = \pi/2$  and  $\varphi = \pi/4$ . Simulated and measured WFs are shown in the upper and lower panels, respectively. Experimental imperfections are not included in the numerical simulations. Since the qubit wave state  $|\psi_w\rangle$  is not orthogonal to the particle state  $|\psi_p\rangle$ , there is some quantum coherence between  $|\alpha\rangle$  and  $|0\rangle$ , even when the test qubit is traced out. As a result, the WF exhibits a strongly nonclassical feature around  $\chi = 1$ , as shown in Fig. 3(a). The measured WF has a minimum value of  $-0.258 \pm 0.030$  at  $\chi = 0.84 - 0.03i$ . In Fig. 3(a), the shapes of the calculated and measured WFs agree well, demonstrating that the measured negative quasi-probabilities are due to quantum interference between  $|\alpha\rangle$  and  $|0\rangle$ . The existence of quantum coherence between these two state components implies that their correlation with the behavior of the test qubit shown in Fig. 2(b) is nonclassical. Without reading out the test qubit's state, the WF is independent of the value of  $\theta$ , since any local unitary operation on the test qubit does not affect the QBS state after their interaction. When the test qubit's state is measured, the minimum value of the WF becomes more negative, implying the enhancement of quantum interference between the active and inactive states of the QBS. We have also measured the corresponding WFs for  $\varphi = \pi/8$  and  $3\pi/8$  (see Fig. S.2 in the Supplementary Material for details). As expected, for both cases there exists a region where the WF has negative values, and the quantum interference is enhanced when the test qubit's state is measured. These results further show that there exists entanglement between the quantum beam-splitter and the test qubit. We note the final QBS-qubit state was realized deterministically and the qubit measurement was done in a single-shot manner. Another benefit of this experimental implementation is that it allows the observation of the transition from a quantum to a classical beam splitter, as shown in the

Supplementary Material.

We have proposed and carried out a quantum delayed-choice experiment for a qubit interacting with a Ramsey interferometer, achieved by preparing one of the two Ramsey beam splitters in a superposition of its active and inactive states. Unlike previous experiments, here the beam splitter is really a quantum object, and the qubit behavior is clearly correlated with the quantum state of this beam splitter, significantly different from situations where an ancilla controls the transformation produced by a classical beam splitter. The quantum nature of the QBS is unambiguously verified by the negative values of its Wigner function. We have also observed variations in the Ramsey fringe contrast and the corresponding negativity of the Wigner function as a function of delay, illustrating the quick damping of the quantum coherence of the QBS. Using qubits with stronger nonlinearity and longer coherence times, we plan to increase the size and fidelity of the cat state and to explore the gradual transition from a quantum to a classical measuring device. This experiment was realized using a circuit QED system; however, similar experiments could be performed using microwave cavity QED [25, 26] or ion-trap setups [27, 28]. We further note that the idea of producing a conditional rotation on a qubit with an oscillator in a mesoscopic superposition may be useful for generation of important entangled states. This conditional dynamics, together with the qubit-oscillator quantum state transfer [29], could be used to produce entanglement between two oscillators. Another example is the generation of entanglement between multiple qubits and an oscillator by performing rotations on these qubits conditional on the oscillator's state.

---

\* Electronic address: t96034@fzu.edu.cn

† Electronic address: martinis@physics.ucsb.edu

‡ Electronic address: anc@uchicago.edu

[1] N. Bohr, in *Quantum Theory and Measurement* (eds J. A. Wheeler and W. H. Zurek ) 9-49 (Princeton University Press, Princeton, NJ, 1984).

[2] M. O. Scully, B. G. Englert, and A. Walther, *Nature* **351**, 111-116 (1991).

[3] B. G. Englert, *Phys. Rev. Lett.* **77**, 2154-2157 (1996).

[4] S. B. Zheng, *Opt. Comm.* **173**, 265-267 (2000).

[5] P. Bertet *et al.*, *Nature* **411**, 166-170 (2001).

[6] J. A. Wheeler, in *Mathematical Foundations of Quantum Mechanics* ( eds A. R. Marlow ) 9-48 (Academic 1978, New York, 1978).

[7] J. A. Wheeler, in *Quantum Theory and Measurement* (eds J. A. Wheeler and W. H. Zurek ) 182-213 (Princeton

University Press, Princeton, NJ, 1984).

[8] A. J. Leggett, in *Compendium of Quantum Physics* (eds D. Greenberger, K. Hentschel, and F. Weinert) 161-166 (Springer, Berlin, 2009).

[9] T. Hellmut, H. Walther, A. G. Zajonc, and W. Schleich, *Phys. Rev. A* **35**, 2532-2541 (1987).

[10] B. J. Lawson-Daku *et al.*, *Phys. Rev. A* **54**, 5042-5047 (1996).

[11] Y. H. Kim, R. Yu, S. P. Kulik, Y. Shih, and M. O. Scully, *Phys. Rev. Lett.* **84**, 1-5 (2000).

[12] V. Jacques *et al.*, *Science* **315**, 966-968 (2007).

[13] X. S. Ma *et al.*, *Nat. Phys.* **8**, 479-484 (2012).

[14] R. Ionicioiu and D. R. Terno, *Phys. Rev. Lett.* **107**, 230406 (2011).

[15] S. S. Roy, A. Shukla, and T. S. Mahesh, *Phys. Rev. A* **85**, 022109 (2012).

[16] R. Auccaise *et al.*, *Phys. Rev. A* **85**, 032121 (2012).

[17] J. S. Tang, Y. L. Li, C. F. Li, and G. C. Guo, *Nat. Photonics* **6**, 600-604 (2012).

[18] F. Kaiser, T. Coudreau, P. Milman, D. B. Ostrowsky, and S. Tanzilli, *Science* **338**, 637-640 (2012).

[19] A. Peruzzo, P. Shadbolt, N. Brunner, S. Popescu, and J. L. O'Brien, *Science* **338**, 634-637 (2012).

[20] H. Lee, P. Kok, and J. P. Dowling, *J. Mod. Opt.* **49**, 2325-2338 (2002).

[21] V. Buzek and P. L. Knight, Quantum interference, superposition states light, and nonclassical effects. *Progress in Optics XXXIV* ed E. Wolf, (Elsevier, Amsterdam, 1995).

[22] W. P. Schleich, *Quantum Optics in Phase Space* (Wiley, Berlin, 2001).

[23] Y. P. Zhong *et al.*, *Nat. Commun.* **5**, 3135 (2014).

[24] M. Hofheinz *et al.*, *Nature* **459**, 546-549 (2009).

[25] M. Brune *et al.*, *Phys. Rev. Lett.* **77**, 4887-4890 (1996).

[26] S. Deléglise *et al.*, *Nature* **455**, 510-514 (2008).

[27] C. Monroe, D. M. Meekhof, B. E. King, and D. J. Wineland, *Science* **272**, 1131-1136 (1996).

[28] C. Hempel *et al.*, *Nat. Photonics* **7**, 630-633 (2013).

[29] B. Vlastakis *et al.*, *Science* **342**, 607 (2013).

**Acknowledgments:** We thank D. J. Wineland for

fruitful discussions. This work was supported by the Major State Basic Research Development Program of China under Grant Nos. 2012CB921601 and 2014CB921200, and the National Natural Science Foundations of China under Grant Nos. 11374054, 11222437, and 11374083. The experiment was performed at Zhejiang University.

## SUPPLEMENTARY INFORMATION FOR 'QUANTUM DELAYED-CHOICE EXPERIMENT WITH A BEAM SPLITTER IN A QUANTUM SUPERPOSITION'

### QUANTUM CIRCUIT AND QUBIT-RESONATOR INTERACTION CONTROL

The quantum circuit used to implement our quantum delayed-choice experiment consists of two phase qubits coupled to a superconducting coplanar waveguide resonator, as shown in Fig. S.1. The sample, as described in Ref. 1, involves four qubits, two of which are not used in our experiment and not shown in the circuit diagram. The resonator has a fixed frequency of 6.205 GHz, while the frequency of each qubit is tunable through a flux bias coil. Neglecting the effects of higher levels of the qubits, the qubit-resonator interaction Hamiltonian in the interaction picture is given by

$$H = \hbar \sum_{j=1}^2 \Omega_j (e^{i\Delta_j t} \sigma_j^+ a + e^{-i\Delta_j t} \sigma_j^- a^\dagger), \quad (S1)$$

where  $\sigma_j^+$  and  $\sigma_j^-$  are the raising and lowering operators for qubit  $j$ ,  $a$  and  $a^\dagger$  the annihilation and creation operators of the field in the resonator, and  $\Omega_j$  is the coupling strength between qubit  $j$  and the resonator with the detuning  $\Delta_j$ . The Hamiltonian describes the coherent energy exchange between the qubits and the resonator. When  $\Delta_j \gg \Omega_j$  the photon transfer probability between qubit  $j$  with the resonator is negligible, implying their interaction is effectively switched off. On the other hand, when  $\Delta_j = 0$  and  $\Delta_k \gg \Omega_k$  ( $j, k = 1, 2$  and  $j \neq k$ ) the interaction between qubit  $j$  and the resonator is described by the Jaynes-Cummings Hamiltonian. The qubit frequency tunability allows us to freely control the qubit-resonator interaction.

### THE FIRST RAMSEY PULSE WITH A COHERENT FIELD IN THE RESONATOR

The coherent field state  $|\alpha\rangle$  stored in the resonator can be expressed as a superposition of photon number states:  $|\alpha\rangle = \sum_{n=0}^{\infty} C_n |n\rangle$ , where  $C_n = \exp(-|\alpha|^2/2) \alpha^n / \sqrt{n!}$  is the probability amplitude for having  $n$  photons. The Rabi oscillation frequency associated with the photon-number state  $|n\rangle$  is  $\sqrt{n}\Omega$ . After an interaction time



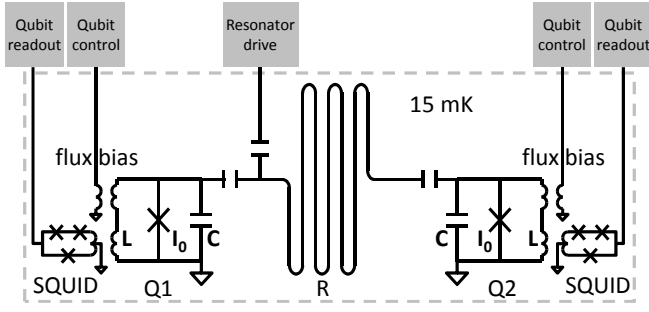


Figure S1: (Color online) Circuit schematic. Two phase qubits are coupled to a superconducting coplanar waveguide resonator via capacitors. The detuning between each qubit and the resonator is adjusted through a flux bias coil, enabling the relevant qubit-resonator interaction to be effectively switched on and off. External microwave pulses are coupled to the qubits through the flux bias coil, and to the resonator through the capacitor on the left side of the resonator. The coupling strengths of the resonator to the two qubits are  $2\pi \times 17.5$  MHz and  $2\pi \times 17.7$  MHz, respectively. The energy relaxation times for these two qubits are 520 ns and 560 ns, respectively, and the Ramsey dephasing times for both qubits are about 150 ns. The energy relaxation time of the resonator is 3.0  $\mu$ s without measurable dephasing.

$t_\alpha = \pi/(4|\alpha|\Omega)$  the state of the qubit-resonator system evolves to

$$|\Psi\rangle = \sum_{n=0}^{\infty} [C_n \cos(\sqrt{n}\Omega t_\alpha)|g\rangle - iC_{n+1} \sin(\sqrt{n+1}\Omega t_\alpha)|e\rangle]|n\rangle. \quad (S2)$$

The coherent field has a Poissonian photon-number distribution, with the mean photon number  $\bar{n} = |\alpha|^2$  and variance  $\Delta n = |\alpha|$ . When the field amplitude is large,  $\Delta n$  is much smaller than  $\bar{n}$ . In this case, we have  $C_{n+1}/C_n = \alpha/\sqrt{n+1} \simeq e^{i\vartheta}$  and  $\sqrt{n}\Omega t_\alpha \simeq |\alpha|\Omega t_\alpha = \pi/4$ , where  $\vartheta$  is the argument of the complex amplitude  $\alpha$ . For  $\vartheta = 0$ , the total state  $|\Psi\rangle$  is approximately a product of the qubit state  $(|g\rangle - i|e\rangle)/\sqrt{2}$  with the field state  $|\alpha\rangle$ .

### EXPERIMENTAL SEQUENCE FOR RAMSEY INTERFERENCE

The state  $|\psi_{b,i}\rangle$  of Eq. (3) of the main text with  $\varphi \neq 0$ ,  $\pi/2$  is generated by coherently pumping photons into the resonator one by one through the ancilla qubit, exploiting an algorithm theoretically proposed in Ref. 2. Experimental implementation of this algorithm in a superconducting resonator involves alternative, well-controlled qubit drive operations and qubit-resonator swap operations, as detailedly described in Refs. 3 and 4 and illustrated in Fig. S2. Here the qubit drive operation is achieved by applying a resonant microwave pulse through the flux bias coil. To decrease the reasonable cutoff in the

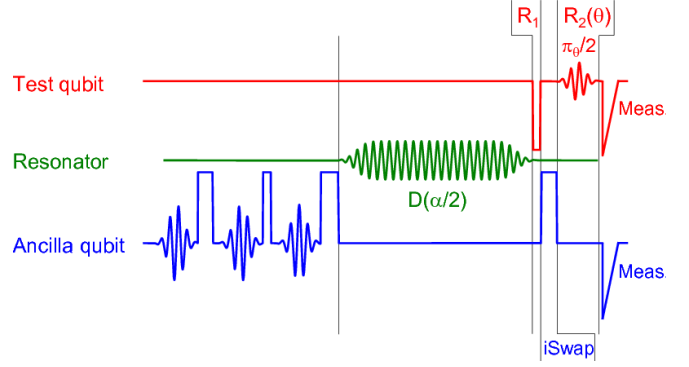


Figure S2: (Color online) Experimental sequence for Ramsey interference. Three microwave pulses (blue sinusoids) and three qubit-resonator swap pulses (blue squares) applied alternately, are used to generate the superposition state  $\mathcal{N}(\cos \varphi |\alpha\rangle - \sin \varphi |0\rangle)$  with  $\alpha = 2$  (the cutoff is  $n = 4$ ) in the resonator. The ancilla qubit returns to its ground state and no further operation is performed on it for measurement of the Ramsey signal of Fig. 2a of the main text. The displacement pulse  $D(\alpha/2)$  further turns the resonator field state into  $|\psi_{b,i}\rangle$  (see Eq. (3) of the main text).  $R_1$  on the test qubit is implemented by turning on the qubit-resonator interaction for a time  $t_\alpha$  (red square), while  $R_2(\theta)$  achieved by applying a phase-tunable, on-resonance microwave pulse to the test qubit (red sinusoid). For different  $\varphi$ , the resulting excited-state probability of the test qubit as a function of  $\theta$  is measured (red triangle pulse), which forms the Ramsey interference pattern, as shown in Fig. 2a of the main text. To distinguish between the wave and particle outcomes as shown in Fig. 2b of the main text, after  $R_1$  the state of the resonator is examined by the ancilla qubit using an iSwap gate (the fourth blue square), followed by ancilla state detection (the blue triangle pulse).

Fock-state expansion, we first generate the supersotian state  $\mathcal{N}(\cos \varphi |\alpha/2\rangle - \sin \varphi |-\alpha/2\rangle)$  with  $\alpha = 2$  (the cutoff is  $n = 4$ ), and then displace it in phase space by an amount  $\alpha/2$ , achieving the state  $|\psi_{b,i}\rangle$ . The displacement operation is performed using a microwave pulse capacitively coupled to the resonator. For  $\varphi = 0$ , we directly generate  $|\psi_{b,i}\rangle$  from the vacuum state by performing the displacement operation  $D(\alpha)$ . We produce the states  $|\psi_{b,i}\rangle$  for  $\varphi = 0, \pi/8, \pi/4, 3\pi/8, \pi/2$ , with the fidelities being  $0.898 \pm 0.023$ ,  $0.702 \pm 0.021$ ,  $0.726 \pm 0.028$ ,  $0.760 \pm 0.017$ , and  $0.992 \pm 0.004$ , respectively.

After preparation of  $|\psi_{b,i}\rangle$ , we achieve the first pulse  $R_1$  by turning on the interaction between the test qubit and the resonator for a time  $t_\alpha$ . For the observation of the Ramsey signal displayed in Fig. 2a of the main text,  $R_1$  is directly followed by a phase-tunable, on-resonance microwave  $\pi/2$  pulse  $R_2(\theta)$  applied to the qubit. For different  $\varphi$ , the Ramsey interference pattern is constructed by measuring the resulting excited-state probability of the test qubit as a function of  $\theta$ . To obtain the result shown in Fig. 2b of the main text, after  $R_1$  an additional iSwap gate is applied to the resonator field and the an-

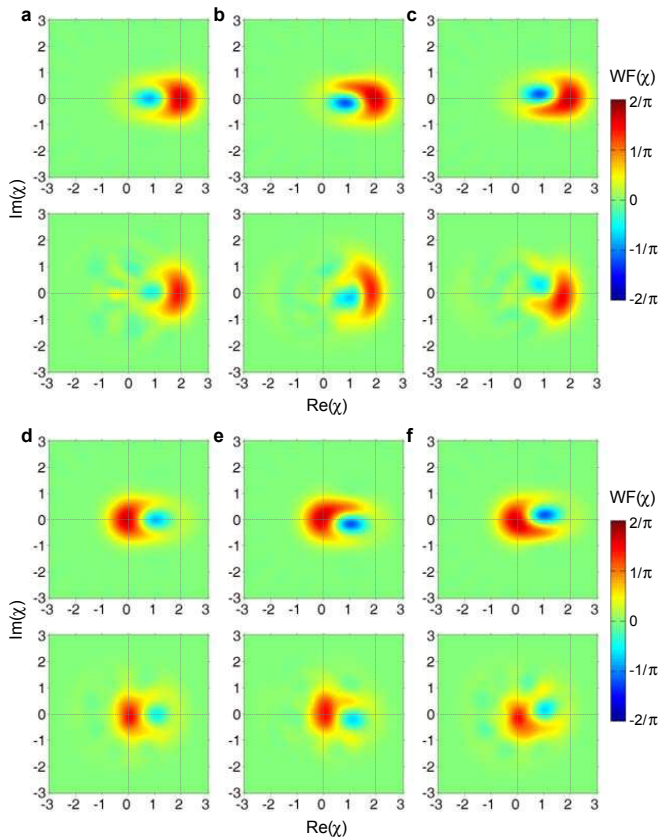


Figure S3: (Color online) Wigner tomography of the quantum beam splitter state. Panels a to c (d to f) display the WFs for  $\varphi = \pi/8$  ( $3\pi/8$ ). The parameters  $\alpha$  and  $\theta$  are as in Fig. 3 of the main text. Shown here are the reconstructed WFs of the resonator field for the three cases from left to right: (a and d) The qubit state is not read-out; (b and e) The qubit is measured in  $|g\rangle$ ; (c and f) The qubit is measured in  $|e\rangle$ . In each panel, the simulated and measured WFs are shown in the upper and lower rows, respectively. Experimental imperfections are not included in numerical simulation. The minimum values of the measured WFs for  $\varphi = \pi/8$  are  $-0.138 \pm 0.020$ ,  $-0.227 \pm 0.021$ , and  $-0.193 \pm 0.024$ , while those for  $\varphi = 3\pi/8$  are  $-0.152 \pm 0.025$ ,  $-0.218 \pm 0.029$ , and  $-0.215 \pm 0.031$ , respectively.

cilla, as shown in Fig. S.2. The wave and particle behaviors of the test qubit is post-selected by detecting the state of the ancilla.

### MEASUREMENT OF WIGNER FUNCTIONS

To reconstruct the WF of the reduced density operator of the resonator field without reading-out the state of the test qubit, we perform the displacement operation  $D(-\chi)$  after the second Ramsey pulse, and then let the ancilla qubit initially in the ground state interact with the resonator field for a variable time  $\tau$ , followed by the measurement of the state of the ancilla. The measured probability  $P_e(\tau)$  for the ancilla being in the excited state,

as a function of  $\tau$ , is used to infer the diagonal elements of the displaced density matrix of the resonator field and hence the value of the WF at point  $\chi$  in phase space [3, 4].

To map out the WF of the resonator field associated with the states  $|g\rangle$  and  $|e\rangle$  of the test qubit, we perform the joint qubit-resonator tomography, which requires reading-out both the test and ancilla qubits simultaneously, as described in Ref. 5.

In Fig. S3, we present the measured WFs of the field state in the resonator for  $\varphi = \pi/8, 3\pi/8$ . Panel a (d) shows the WFs when the qubit state is traced out, while b (e) and c (f) exhibit the WFs associated with the outcomes  $|g\rangle$  and  $|e\rangle$  for  $\varphi = \pi/8$  ( $3\pi/8$ ), respectively. In each panel, the simulated and measured WFs are shown in the upper and lower rows, respectively. Experimental imperfections are not included in numerical simulation. As expected, due to the quantum coherence between the present and absent states of the QBS the WF for each case exhibits a nonclassical feature around  $\chi = 1$ . When the qubit state is measured, the quantum interference and hence the negativity of the WF are enhanced. These results, together with those shown in Fig. 2 of the main text, reveal the quantum nature of the QBS for a wide range of the parameter  $\varphi$ .

### OBSERVING TRANSITION FROM QUANTUM TO CLASSICAL BEAM SPLITTER

Another benefit of this experimental implementation is that it allows the observation of the transition from a quantum to a classical beam splitter. To demonstrate this, we now delay the interaction between the test qubit and the resonator for a time  $T$  after the QBS has been prepared in the cat state  $|\psi_{b,i}\rangle$ . Then, just before the test qubit-resonator interaction, the field density operator is given by [6]

$$\rho_b = \mathcal{N}^2 [\cos^2 \varphi |\alpha'\rangle\langle\alpha'| + \sin^2 \varphi |0\rangle\langle 0| - \frac{1}{2} e^{-|\alpha'|^2(1-\epsilon^{-\gamma T})/2} \sin(2\varphi) (|\alpha'\rangle\langle 0| + |0\rangle\langle\alpha'|)], \quad (\text{S3})$$

where  $\alpha' = \alpha e^{-\gamma T/2}$  and  $\gamma$  is the decay rate of a photon in the resonator; we have ignored imperfections in the cat state preparation. In our experimental setup the single-photon lifetime is  $\tau = 1/\gamma \simeq 3.0 \mu\text{s}$ . The qubit-resonator interaction time is set to  $t_{\alpha'} = \pi/(4\alpha'\Omega)$ , so that after  $R_2(\theta)$  the state component  $|\alpha'\rangle|g\rangle$  approximately evolves to  $|\alpha'\rangle|\psi_w\rangle$ , while  $|0\rangle|g\rangle$  evolves to  $|0\rangle|\psi_p\rangle$ .

In Fig. S4(a) we display the measured Ramsey interference signals for  $\varphi = \pi/4$  with different delays  $T$ , showing that the fringe contrast is insensitive to the field decay, as expected. However, the quantum coherence between the active and inactive states of the QBS degrades much faster due to decoherence. Figure S4(b) shows the negative-valued minimum value of the WF as a function



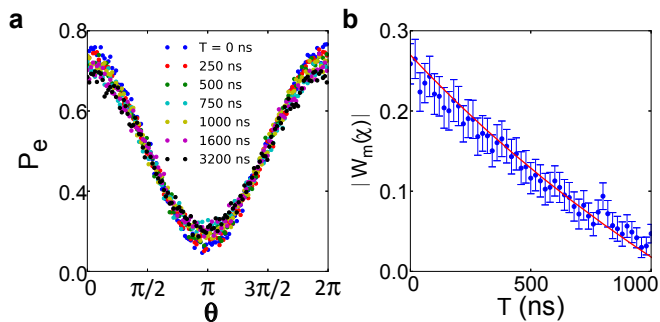


Figure S4: (Color online) Transition from a quantum to a classical beam splitter. (a) Measured Ramsey signals for different delays  $T$ , defined as the interval between the end of the cat state preparation and the start of the qubit-resonator interaction. The parameters are the same as those in Fig. S3. (b) Absolute value of the negative-valued minimum of the WF of the QBS state after  $R_2$ , without reading out the test qubit state, displayed versus  $T$ . The damping of the quantum coherence of the QBS is characterized by the decrease in the negativity of the WF. Error bars indicate the statistical variance. The line is a master-equation simulation taking the prepared cat state as the initial state for the decoherence evolution. The resonator single-photon lifetime is around  $3.0 \mu\text{s}$ , with negligible pure dephasing.

of delay  $T$ , with the WF measured after  $R_2(\theta)$  but without reading out the test qubit state. The blue symbols are the measured results, whereas the red curve represents the simulated decay, taking the prepared cat state as the initial state. For  $\gamma T = 1/3$ , the amplitude of the coherent field is reduced by only 15%, but the absolute value of the minimum of the WF decays almost to zero,

revealing the quick damping of the quantum coherence, which can be defined as the sum of the off-diagonal elements of the third term of Eq. (S3) in the photon-number representation [7]. Equation (S3) predicts that the quantum coherence is shrunk by a factor of about 0.51 after this delay. With a cat state of larger size and higher fidelity, as has been achieved in [3, 4, 8, 9], one could observe further decay of the quantum coherence of the QBS.

\* Electronic address: t96034@fzu.edu.cn

† Electronic address: martinis@physics.ucsb.edu

‡ Electronic address: anc@uchicago.edu

[1] Y. P. Zhong *et al.*, *Nat. Commun* **5**, 3135 (2014).

[2] C. K. Law and J. H. Eberly, *Phys. Rev. Lett.* **76**, 1055 (1996).

[3] M. Hofheinz *et al.*, *Nature* **459**, 546 (2009).

[4] H. Wang *et al.*, *Phys. Rev. Lett.* **103**, 200404 (2009).

[5] X. Y. LinPeng *et al.*, *New J. Phys.* **15**, 125027 (2013).

[6] S. J. D. Phoenix, *Phys. Rev. A* **41**, 5132-5138 (1989).

[7] S. Deléglise *et al.*, *Nature* **455**, 510-514 (2008).

[8] G. Kirchmair *et al.*, *Nature* **495**, 205-209 (2013).

[9] B. Vlastakis *et al.*, *Science* **342**, 607 (2013).